Supporting Information for "Spatio-temporal patterns of Chaos in the Atlantic Overturning Circulation"

Q. Jamet[1], W. K. Dewar[1], N. Wienders[1]and B. Deremble[2]

[1]Department of Earth, Ocean and Atmospheric Science, the Florida State University, Tallahassee, Florida

[2]Laboratoire de Météorologie Dynamique, Paris, France

Contents of this file

1. Model configuration
2. Initial conditions
3. Time processing
4. Comparing the simulated and observed AMOC at 26.5°N

Model configuration The 24-member ensemble simulation is performed with a regional configuration of the Massachusetts Institute of Technology General Circulation Model (MITgcm, Marshall et al., 1997). The vertical discretization (i.e. 46 layers) matches the ORCA12.L46-MJM88 (Molines et al., 2014) configuration used to derive open boundaries.

Corresponding author: Q. Jamet, Department of Earth, Ocean and Atmospheric Science, the Florida State University, Tallahassee, Florida. (qjamet@fsu.edu)

The atmospheric forcing derives from a reanalysis product combined with a use of a one-dimentionnal atmospheric layre mode (CheapAML, Deremble et al., 2013). The employed reanalysis products (DFS4.4, Brodeau et al., 2010; Dussin et al., 2016) is developed by the DRAKKAR project ("drakkar", http://www.drakkar-ocean.eu) based on a combination of the ERA-40 reanalysis and satellite observations. In CheapAML, atmospheric surface temperature and relative humidity respond to ocean surface structures, but other variables (downward longwave and solar shortwave radiation, precipiations) are prescribed. To match the 6-hour time resolution of prescribed atmospheric winds, we construct a diurnal cycle in solar shortwave radiation such that the short waves are zero at 6 am and 12 am, and the daily values are doubled at 12 pm and 6 pm. Daily downward longwave radiation is linearly extrapolated in time to 6-hourly field. We also use daily precipitations from DFS5.2 (Dussin et al., 2013, 2016) because of its better time resolution (monthly fields in DFS4.4). Precipitations are also linearly extrapolated to 6-hourly fields. From the spun-up oceanic state of January 1st 1958 derived from the ORCA12.L46-MJM88 configuration, the model is integrated for 5 years (1958-1962) to minimize the effects of a shock due to the initialization of the model. It is then integrated forward in time for 50 years over the period 1963-2012 with a 24-member ensemble strategy.

Fig. S1 provides an overview of the large scale mean circulation simulated by our 1/12° North Atlantic regional configuration. The time mean Sea Surface Height (SSH) exhibits a realistic large scale gyre organization, with a separation between the subtropical and the subpolar gyre that takes place around 40°N. In the Gulf of Mexico, we note the presence of the loop current structure northwestward of Cuba. The SSH time mean

structure is associated with surface currents, notably the Gulf Stream flowing along the east coast of Florida with velocities reaching 2 m s^{-1}, and separating from the coast downstream of Cap Hatteras. Note that the Gulf Stream separation takes place slightly more north than usually found in ocean models at that resolution (Chassignet et al., Chassignet2017; Schoonover et al., 2017) and in observations (Andres, 2016). In the interior, the 2-dimensional structure of the time mean Atlantic Meridional Overturning Circulation (AMOC, Fig. 1) exhibits a spatial pattern similar to what is usually simulated by ocean and climate models. It consists in a positive upper cell peaking at 18 Sv (1 Sv = 10^6 m^3 s^{-1}) at 38°N and 1000 m depth, and a negative cell below 3000 m. Further comparisons between the simulated and the observed AMOC at 26.5°N are discussed below.

Initial conditions After the 5 years spin-up period (1958-1962), the 24 initial conditions used to generate the ensemble have been computed as follows: during an initial month long integration beginning January 1, 1963, 12 ocean states separated in time by 48 hours were extracted. These were used to reinitialize 12, 1-year long runs conducted under a repeating 1963 forcing where January, 1st was replaced by the ocean state of the aforementioned extracted days. The model states on January 1st of the following year were used as the initial conditions to run the 12 first ensemble members, starting from January 1st 1963. The same procedure was used to generate the 12 last ensemble members initial conditions, where the 1-year long runs were initialized with 2-days apart ocean states from December, 1962 instead. The one-year integration is sufficient to decorrelate the mesoscale variability, and our integration strategy insures the initial conditions are consistent with

the upcoming 1963 forcing. The resulting spread of the 24 initial conditions are the results of the growth of small, dynamically consistent perturbations. We have verified that this spread is consistent with another strategy found in the literature (Germe et al., 2017), where a Gaussian white noise with a standard deviation of 3.5×10^{-3} K was added to the 3-dimensional temperature oceanic field and the resulting perturbed oceanic temperature was used to initiate a one-year run conducted under a repeating 1963 forcing.

Time processing To compute the intrinsic-to-total variance ratio and perform both the Principal Component Analysis and the regression analysis, the 5-d averaged model AMOC has been high-pass filtered using a nonlinear second-order local regression method (LOESS, Cleveland et al., 1988) with a 50-year cut-off period. This insures that low frequency signals, such as long term trends, model drift or unresolved natural low frequency variability, as well as the 50-year time mean, are discarded for the analysis. An example of the nonlinear detrending procedure is given on Fig. S2 for the AMOC time series at 26.5°N and 1200 m. Consistent with the annual-mean AMOC variations found in most of the ocean-only models of the CORE-II experiments (cf Fig. 1 of Danabasoglu et al., 2016), the simulated AMOC maximum at the RAPID location is weaker by a few Sverdrups at the biginning of the simulations compared to its 1963-2012 time mean, peaks in the mid- 1990s to about +3 Sv and decreases afterward. The nonlinear trends computed from the LOESS method (light blue line) remove this very low frequency AMOC signal unresolved by the too short duration of the simulations.

To assess the effects of this high-pass filter on the spectrum of a 50-year long time series, we have performed a sensitivity test with synthetic time series. We have first constructed

a 600-year long time series as a pure white noise signal with a 5-day temporal resolution. Then, we have split this time series into 12 50-year long segments. The ensemble mean Power Spectral Density (PSD) is shown on Fig. S3 (blue line). Then we applied the high-pass filter to the 12 50-year long time series, and compared the ensemble mean PSD of the filtered data (Fig. S3, red line) with the original one. It indicates that the attenuation induced by the high-pass filter at low frequency is smaller than -2 dB for periods shorter than 30 years, suggesting than any signal with a period smaller than 30 years can be considered as unfiltered.

To focus on interannual and longer timescales, the detrended filtered data have also been low-pass filtered with a forward and reverse Butterworth 10^{th} order digital low-pass filter with a cutoff period of 1 year. This aims to remove high frequency signals that are likely to mask the longer timescales of interest. Fig. S4 shows the impact of time filtering on the intrinsic-to-total variance ratio, i.e. increasing the ratio all over the domain as a result of the filtering. Here, we have employed low-pass filters with a range of cut-off frequencies, in order to study the effects of the filtering. Note that at the RAPID location, the ratio R peaks at about 45% for a $\frac{1}{2}$-year cut-off period, and reduces for longer periods, suggesting the presence of sub-annual intrinsic variability. The analysis presented in the article uses a one year cut-off, which produces slightly lower R ratios at the RAPID site. We find the applied processing damps variance on time scales comparable to 1 year (green line of Fig. S3), such that only the unaffected time scales longer than 2 years are considered in the analysis. Note that this procedure only partially removes the

seasonal cycle, requiring that a seasonally varying climatological mean computed from the ensemble mean is subtracted prior to the application of the low-pass filter.

Comparing the simulated and observed AMOC at 26.5°N Data from the RAPID-MOCHA-WBTS program (McCarthy et al., 2015) have been retrieved online at http://www.rapid.ac.uk/rapidmoc/rapid_data/datadl.php. The 12-hourly, 2-d low-pass filtered overturning streamfunction from April 1st 2004 to December 31^{st} 2012 has been reprocessed into 5-day averages, and vertically interpolated onto the 46 levels model grid in order for both data sets to have the same time and spatial resolution. This interpolation induces small enough changes in volume transport to be considered as conservative, and no biases in the model-observations comparison are expected. The modeled AMOC has been computed by zonally integrating the 5-day averaged model output meridional velocities across the North Atlantic, from Florida to the west coast of Africa, and vertically from the bottom toward the surface. Note that this definition slightly differs from the one used to compute the AMOC in the latitude-depth plane, where the latter includes the Gulf of Mexico. We have verified that both computations lead to identical overturning estimations in term of time mean structure and in the frequency band of interest. No-slip boundary conditions were applied at the ocean eastern boundary and at the bottom. Unlike the RAPID-MOCHA-WBTS analysis (McCarthy et al., 2015), we do not impose a zero net meridional flow in our calculation. Instead, the net transport is imposed by the net volume transport across the northern and southern open boundaries (of about 1 Sv flowing southward on average, and thought to reflect the Bering Strait inflow). We have

tested our analysis calculating a similar mass flux corrected AMOC and found our results unaffected.

Fig. S6 shows the vertical structure of the time mean AMOC for the 2004-2012 period for the ensemble mean model outputs (black) and for the observations (red). The simulated time mean AMOC at 26.5°N underestimates the observations, but the model-data misfit remains in the range of uncertainties usually found in ocean-only models (cf Fig. 5 of Danabasoglu et al., 2014), the latter being mostly attributed to model parameter choices. This misfit results from combined effects of a weak northward flowing Florida Current (FC) and a strong southward flowing Western Boundary Current (WBT) (Fig. S7). The time mean FC at 26.5°N is underestimated by about 10 cm s^{-1} compared to observations (Leaman et al., 1987), leading to a time mean transport (28 Sv) which is weaker by about 4 Sv compared to the observed long-term mean (Meinen et al., 2010). The upper part (above 600 m) of the time mean WBC at 26.5°N matches with observations, but its lower part is overestimated by about 5 cm s^{-1}, leading to a southward transport along the boundary that is several Sverdrups larger than observational estimates (Bryden et al., 2005).

References

Andres, M. (2016). On the recent destabilization of the gulf stream path downstream of cape hatteras. *Geophys. Res. Lett.*, *43*(18), 9836–9842.

Brodeau, L., Barnier, B., Treguier, A.-M., Penduff, T., & Gulev, S. (2010). An ERA40-based atmospheric forcing for global ocean circulation models. *Ocean Modelling*,

31(3-4), 88–104.

Bryden, H., Johns, W. E., & Saunders, P. M. (2005). Deep western boundary current east of abaco: Mean structure and transport. *J. Mar. Res.*, *63*(1), 35–57.

Chassignet, E. P., & Xu, X. (2017). Impact of horizontal resolution (1/12 to 1/50) on gulf stream separation, penetration, and variability. *J. Phys. Oceanogr.*, *47*(8), 1999–2021.

Cleveland, W. S., & Devlin, S. J. (1988). Locally weighted regression: an approach to regression analysis by local fitting. *Journal of the American statistical association*, *83*(403), 596–610.

Danabasoglu, G., Yeager, S. G., Bailey, D., Behrens, E., Bentsen, M., Bi, D., ... others (2014). North Atlantic simulations in coordinated ocean-ice reference experiments phase II (CORE-II). Part I: mean states. *Ocean Modelling*, *73*, 76–107.

Danabasoglu, G., Yeager, S. G., Kim, W. M., Behrens, E., Bentsen, M., Bi, D., ... others (2016). North Atlantic simulations in Coordinated Ocean-ice Reference Experiments phase II (CORE-II). Part II: Inter-annual to decadal variability. *Ocean Modelling*, *97*, 65–90.

Deremble, B., Wienders, N., & Dewar, W. (2013). Cheapaml: A simple, atmospheric boundary layer model for use in ocean-only model calculations. *Mon. Wea. Rev.*, *141*(2), 809–821.

Dussin, R., & Barnier, B. (2013). *The making of DFS 5.1. Drakkar Project Rep.* [available online at http://www.drakkar-ocean.eu/publications/reports/dfs5-1-report].

Dussin, R., Barnier, B., Brodeau, L., & Molines, J. (2016). The making of the drakkar forcing set dfs5. *DRAKKAR/MyOcean Rep. 01–04*, *16*.

Fairall, C., Bradley, E. F., Hare, J., Grachev, A., & Edson, J. (2003). Bulk parameterization of air–sea fluxes: Updates and verification for the coare algorithm. *J. Clim.*, *16*(4), 571–591.

Germe, A., Sévellec, F., Mignot, J., Swingedouw, D., & Nguyen, S. (2017). On the robustness of near term climate predictability regarding initial state uncertainties. *Climate dynamics*, *48*(1-2), 353–366.

Leaman, K. D., Molinari, R. L., & Vertes, P. S. (1987). Structure and variability of the florida current at 27 n: April 1982–july 1984. *J. Phys. Oceanogr.*, *17*(5), 565–583.

Marshall, J., Adcroft, A., Hill, C., Perelman, L., & Heisey, C. (1997). A finite-volume, incompressible Navier Stokes model for studies of the ocean on parallel computers. *J. Geophys. Res.*, *102*(C3), 5753–5766.

McCarthy, G., Smeed, D., Johns, W., Frajka-Williams, E., Moat, B., Rayner, D., ... Bryden, H. (2015). Measuring the atlantic meridional overturning circulation at 26 n. *Progress in Oceanography*, *130*, 91–111.

Meinen, C. S., Baringer, M. O., & Garcia, R. F. (2010). Florida current transport variability: An analysis of annual and longer-period signals. *Deep Sea Research Part I: Oceanographic Research Papers*, *57*(7), 835–846.

Molines, J., Barnier, B., Penduff, T., Treguier, A., & Le Sommer, J. (2014). *Orca12. l46 climatological and interannual simulations forced with dfs4. 4: Gjm02 and mjm88. drakkar group experiment rep* (Tech. Rep.). GDRI-

DRAKKAR-2014-03-19, 50 pp.[Available online at http://www. drakkar-ocean. eu/publications/reports/orca12_reference_experiments_2014.].

Schoonover, J., Dewar, W. K., Wienders, N., & Deremble, B. (2017). Local sensitivities of the gulf stream separation. *J. Phys. Oceanogr.*, *47*(2), 353–373.

Xu, X., Schmitz, W., Hurlburt, H., & Hogan, P. (2012). Mean atlantic meridional overturning circulation across 26.5 n from eddy-resolving simulations compared to observations. *Journal of Geophysical Research: Oceans*, *117*(C3).

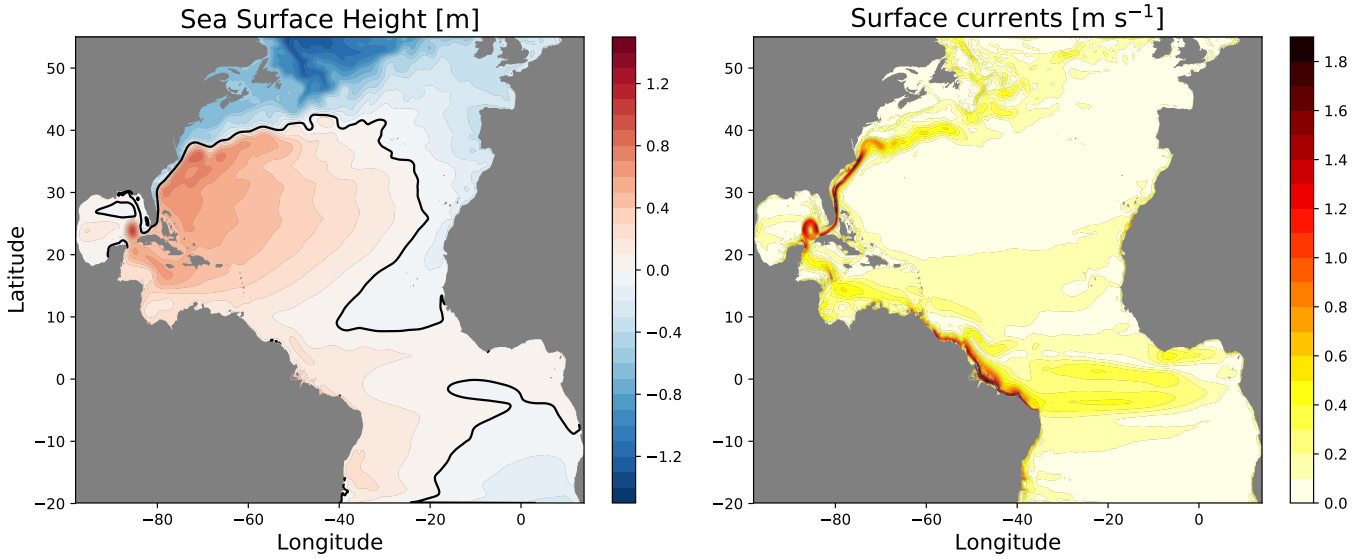

Figure S1. Time mean Sea Surface Height (SSH, left) and surface currents (right) simulated by our 1/12° horizontal resolution North Atlantic regional configuration.

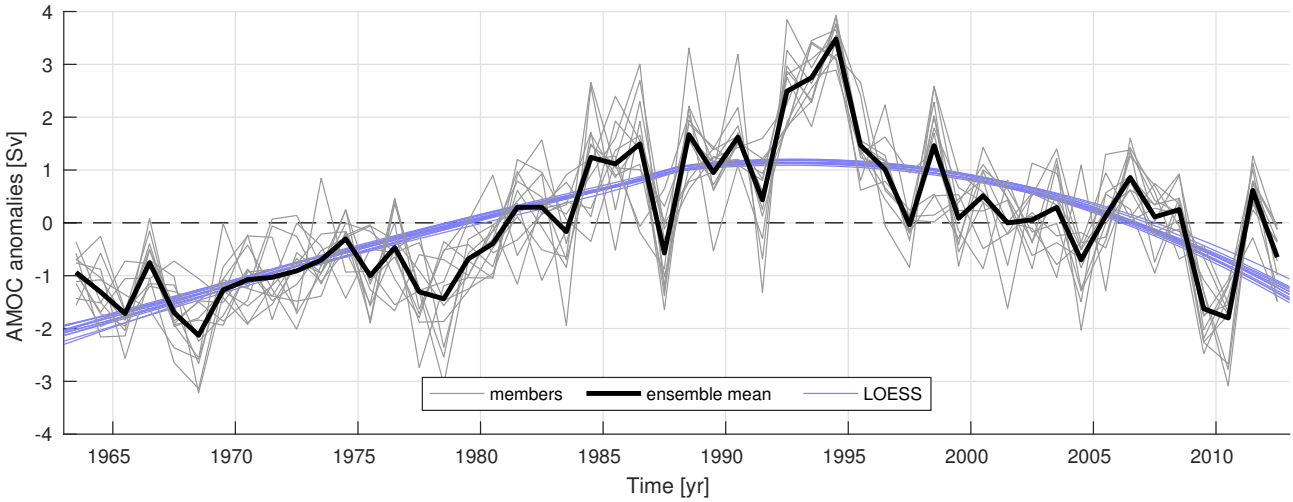

Figure S2. Undetrended modeled AMOC annual-mean anomaly time series at 26.5°N and 1200 m for the 1963-2012 period. The annual-mean AMOC anomalies for each members (gray) and for the ensemble mean (black) are consistent with the low frequency variability usually found in ocean-only model (cf Fig. 1 of Danabasoglu et al., 2016), with a maximum peaking in the mid- 1990s. The nonlinear trends computed from the LOESS method (light blue) remove this very low frequency AMOC signal unresolved by the too short duration of the simulation.

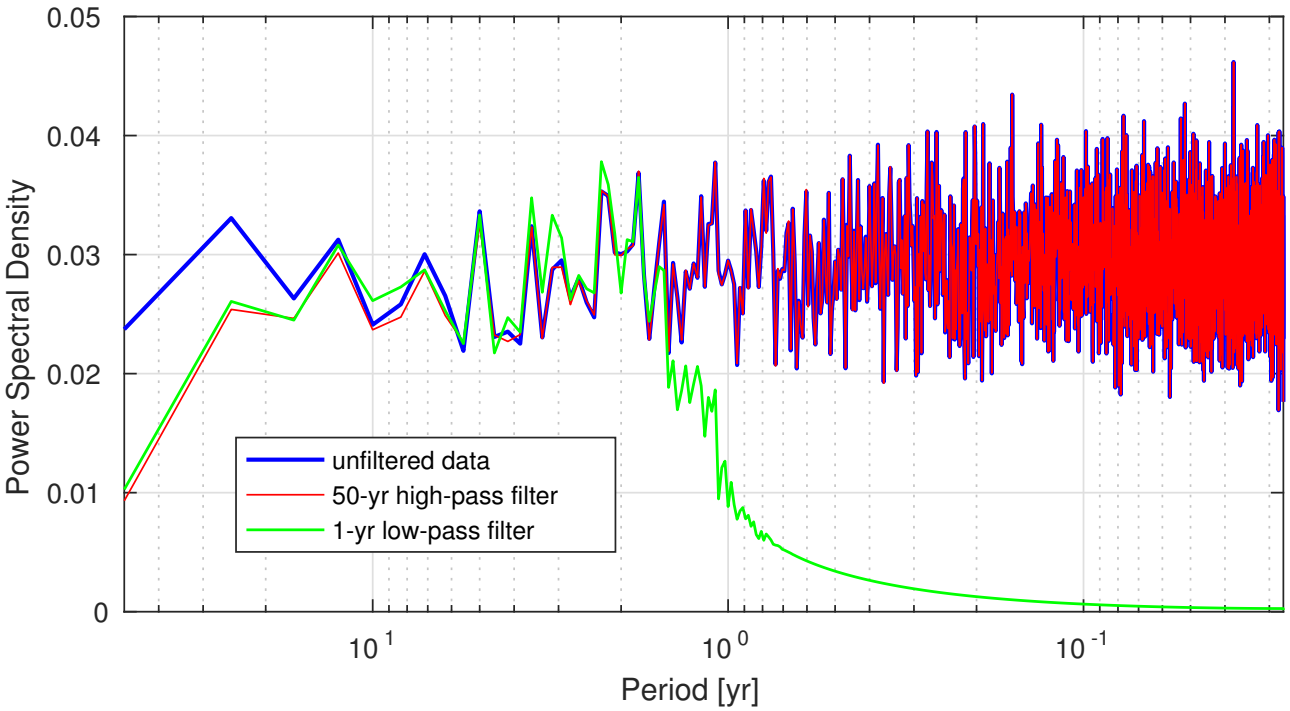

Figure S3. Power Spectral Density of a white noise signal, obtained by splitting a 600 years long time series into 12 time series of 50 years each and averaging their resulting periodograms together, before (blue) and after (red) the application of a 50-yr cut-off period high-pass filter, and after the application of a 1-yr cut-off low-pass filter (green).

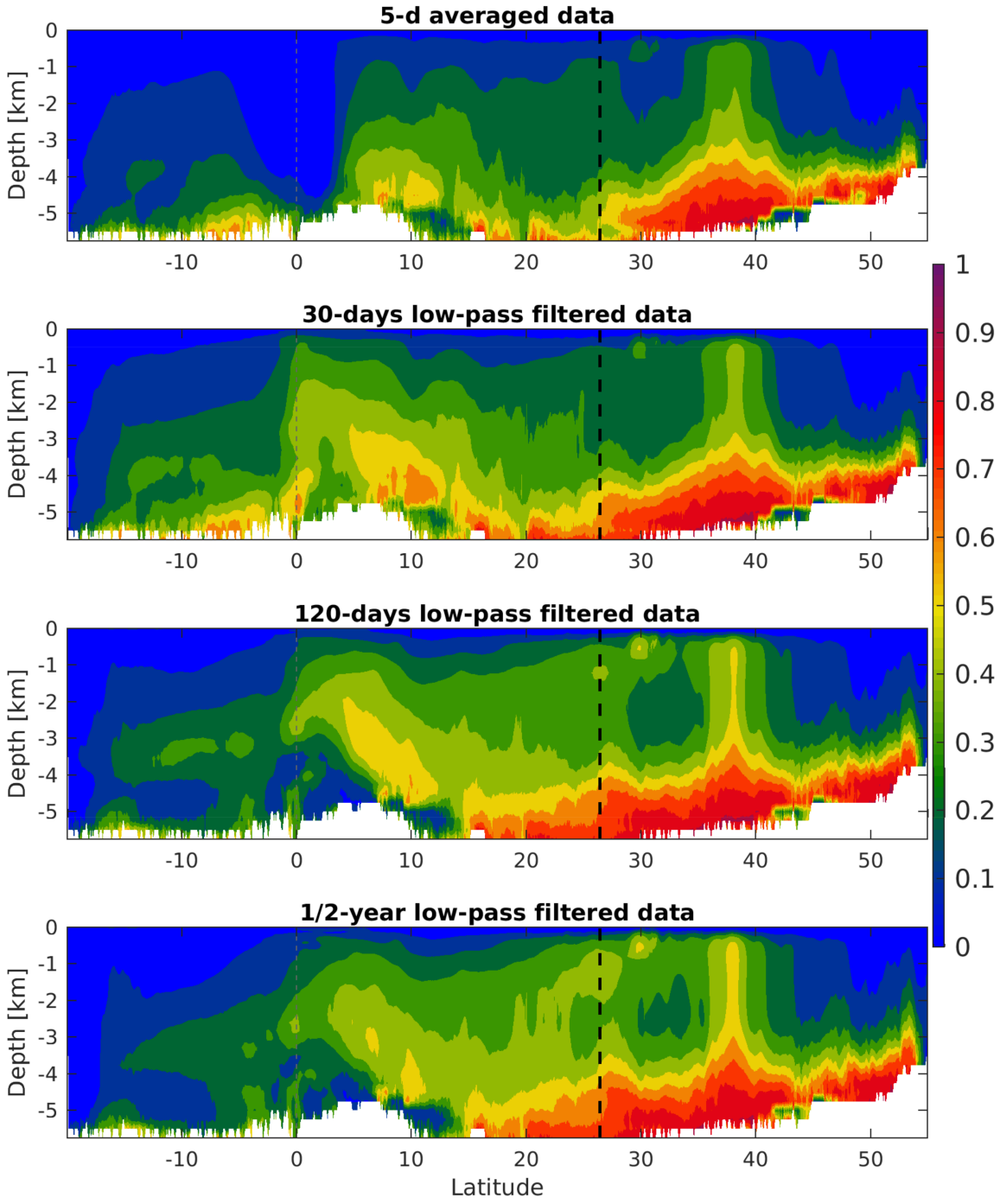

Figure S4. Intrinsic-to-total AMOC variance ratio $R = \frac{\sigma_I^2}{\sigma_T^2}$ function of the cut-off period of the low-pass filter. The AMOC time series have been high-pass filtered before computation, and a yearly repeated seasonal cycle has been removed.

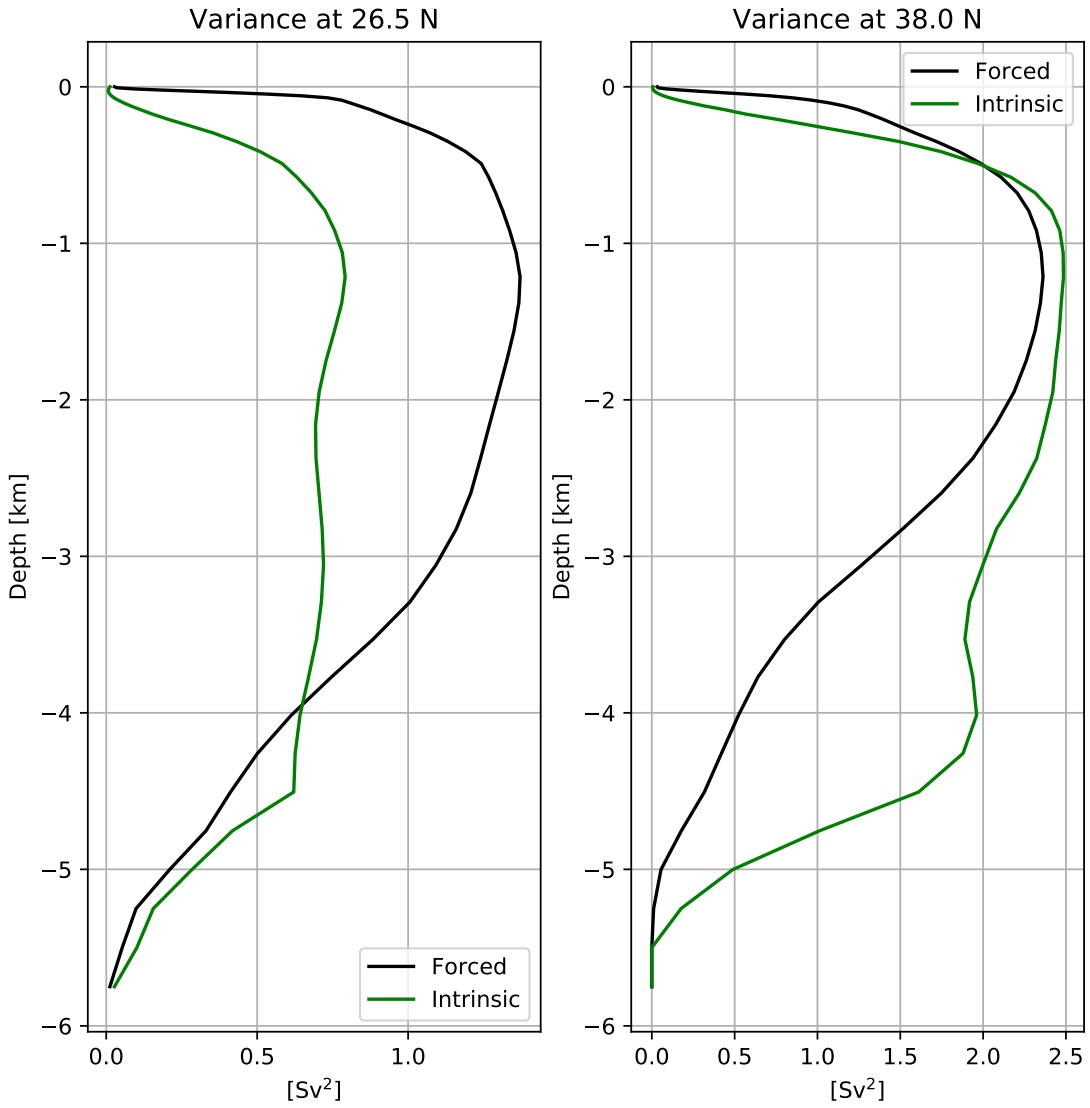

Figure S5. Vertical structure of forced (black) and intrinsic (green) variance at 26.5°N (left) and 36.9°N (right). Time series have been time processed following the same procedure used to obtaine intrinsi-to-total variance ratio of Fig. 1 in the main text.

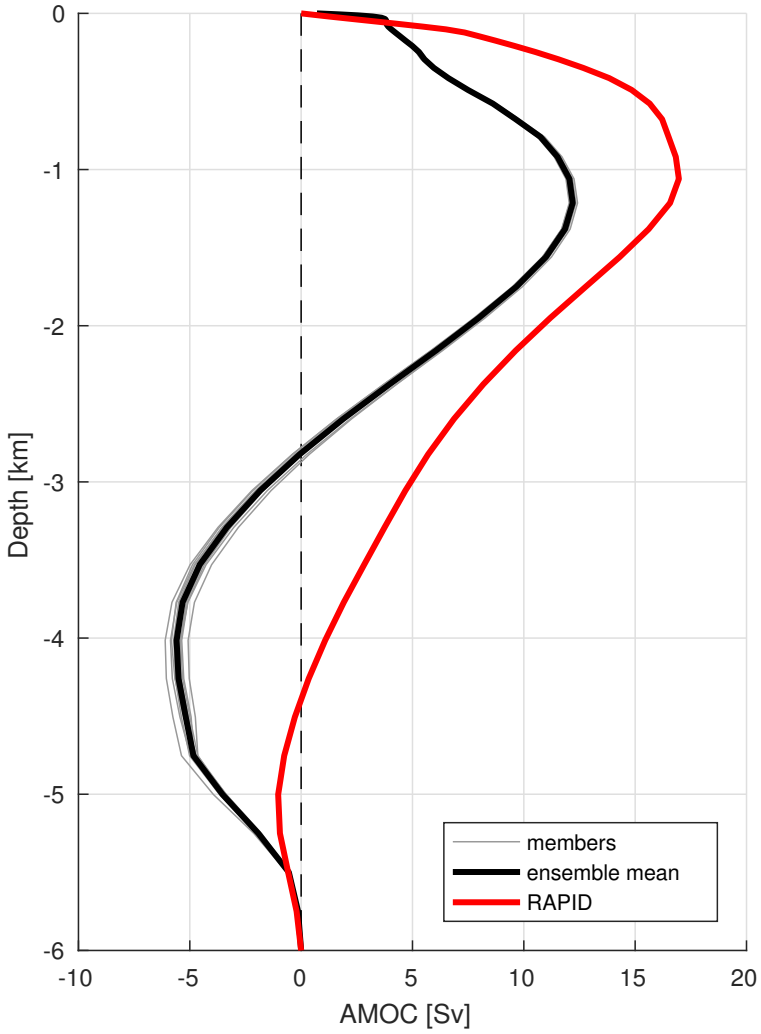

Figure S6. 2004-2012 time mean vertical structure of the AMOC at 26.5°N for each ensemble members (gray), for the ensemble mean (black) and for RAPID observations (red).

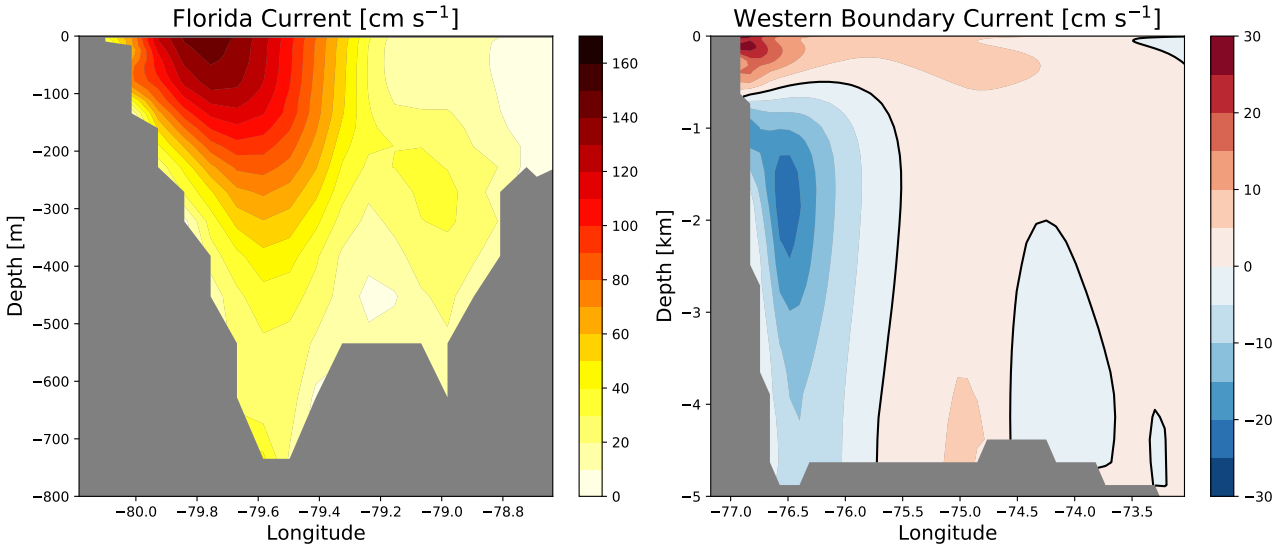

Figure S7. Time mean model northward velocities at 26.5°N for the Florida Current (FC, left) and for the Western Boundary Current (WBC, right).

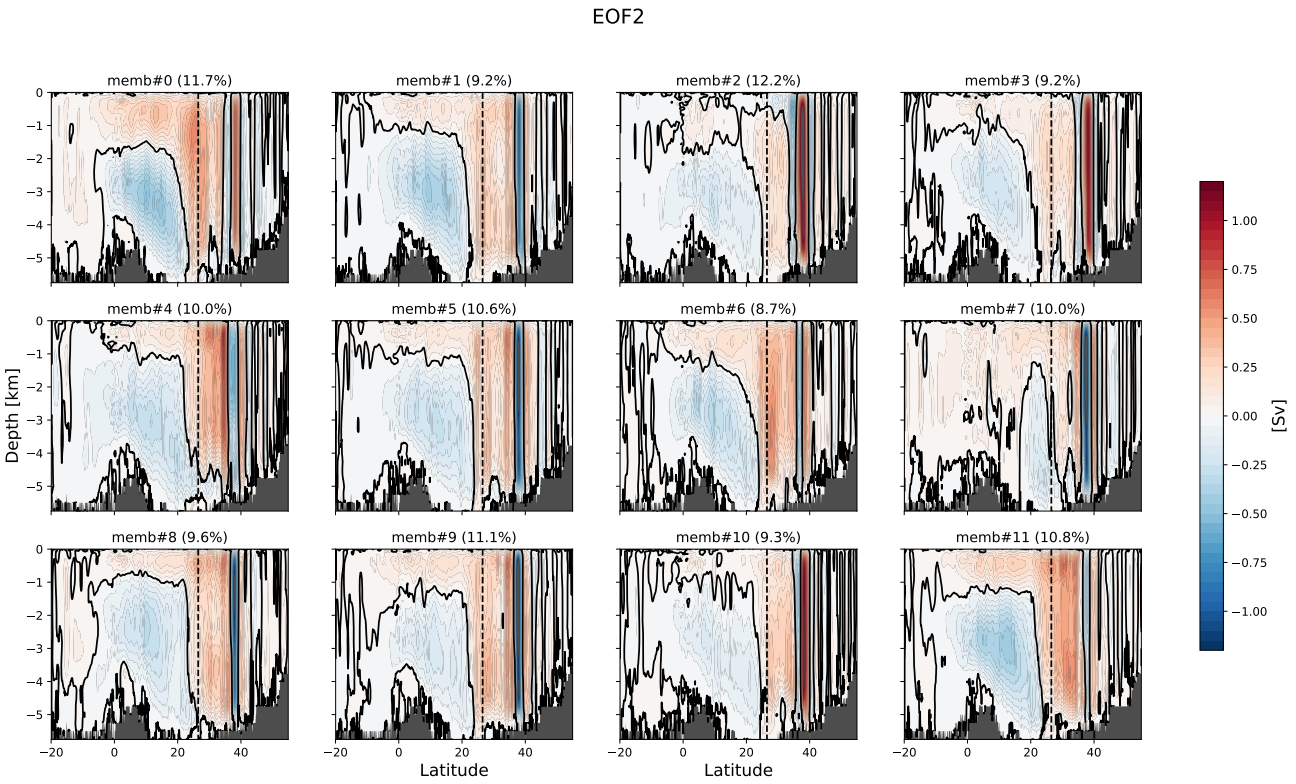

Figure S8. Second Empirical Orthogonal Function (EOF) of the intrinsic variability simulated by each of the 12 first members of the ensemble. The associated explained variance is shown on top of each panel. This figure illustrates the presence of an intrinsic variability near the Gulf Stream separation (38°N) in the EOFs of individual members, which cancel out though ensemble averaging.